

OPTICAL PROPERTIES OF SPIRAL GALAXIES WITH STRONG NUCLEAR RADIO SOURCES: ACTIVE NUCLEI, STARBURSTS, AND COMPOSITE OBJECTS

WILLIAM C. KEEL

Kitt Peak National Observatory¹

Received 1982 November 9; accepted 1984 January 4

ABSTRACT

New optical spectrophotometry, accurate positions, and narrow-band emission-line images have been obtained for the nuclei of spiral and irregular galaxies containing strong radio sources. The optical data support a general division of these objects into those powered by star formation and those dominated by nonthermal processes. In several cases, however, nuclei are classified differently from radio and optical properties, suggesting a composite nature for some nuclei. Further work on this group could indicate whether the two processes are causally related and in which direction.

All these nuclei show emission lines, systematically stronger than in a sample of optically selected nuclei. The emission-line spatial distributions, in most cases, are much like those in normal (optically selected) nuclei. Correlations between emission-line and 6 cm luminosities are explored for each class of nucleus. A correlation with [N II] luminosity for (optically) non-stellar-powered nuclei suggests a common energy source for the emission-line region and the radio emission, while uncertainties in optical reddening obscure any relation for nuclear H II regions.

Subject headings: galaxies: nuclei — galaxies: stellar content — radiation mechanisms —
radio sources: galaxies

I. INTRODUCTION

With few exceptions, the galaxies identified with very luminous radio emission are ellipticals. To date, all galaxies with classical double-lobed radio sources are ellipticals, at least in underlying structure. This fact has figured prominently in many attempts to model the double-lobed sources.

While less luminous than the classical doubles, some spirals have much stronger nuclear radio emission than the average. Study of these galaxies is of interest as a way to understand ways of producing large radio luminosities which might differ from those operating in ellipticals and could be related to the nuclear phenomena observed at other wavelengths.

High-resolution radio maps are now available for many of these “radio-loud” spirals. The physical interpretation of the radio emission is somewhat ambiguous in the absence of additional information. The aftermath of a burst of star formation, with particle acceleration in supernova remnants, is favored in many nuclei, but others show clear evidence of activity not associated with star formation. Optical observations are capable of discriminating between various nuclear processes, using the diagnostics of spectroscopy to study the properties of both the gas and the stars in these nuclei. This is particularly important in distinguishing among various modes of energy input to the gas (starlight, nonstellar radiation, or shock heating, for example). Emission-line images can show whether similar distributions are seen optically and in the radio, especially in early-type galaxies in which dust in the nuclei is not important, and strengthen the identification of emission features with the nuclei themselves. In general, optical data on radio-selected nuclei will complement results from studies of optically complete samples in obtaining a clearer picture of nuclear activity and star formation in spirals.

This paper presents the results of optical spectroscopy and

narrow-band imaging of a sample of spiral galaxies with strong nuclear radio emission. The properties deduced from these data are compared with those of optically selected samples of spirals similarly observed and are examined for correlations with properties of the radio emission.

II. OBSERVATIONS

a) Sample Selection

The galaxies observed in this program were taken from several radio surveys. Eleven are from Condon’s (1980) list of spiral and irregular galaxies with radio-to-optical “flux ratio” $R > 50$. An additional 19 are from the statistically complete samples of Condon *et al.* (1982, hereafter CCGP). These 30 form complete samples of all spirals in the Uppsala catalog ($\delta > -2^\circ 30'$, $m_p \leq 14.5$) for which $R > 50$ in the 2380 MHz Arecibo survey (sample A of CCGP), of spirals with $R > 125$ from Hummel’s (1980) 1415 MHz survey (their sample B), and spirals in Hummel’s survey with 1415 MHz nuclear fluxes above 90 mJy (their sample C); in all of these, galaxies with optically invisible nuclei are omitted here. As noted by CCGP, the different R limits from these two surveys constitute nearly the same limit at a given frequency, because the difference is nearly the average flux ratio from 1415 to 2380 MHz for these galaxies. High-resolution mapping (Condon 1980; CCGP) has confirmed that the high R values in these galaxies result from nuclear emission.

Two galaxies (NGC 6240 and IC 4553) were observed even though their morphologies are irregular rather than spiral. NGC 6240 possesses a Seyfert nucleus or closely related object. The surface brightness of IC 4553 is so low that the available spectra do not allow a useful spectroscopic classification, so it does not appear in the analyses of § III.

The radio properties of the nuclei included in the observing program are summarized for convenience in Table 1. This lists the peak position, half-intensity size (minor axis where

¹ Operated by the Association of Universities for Research in Astronomy, Inc. under contract with the National Science Foundation.

TABLE 1
RADIO PROPERTIES OF SPIRAL GALAXY NUCLEI

Name	Type	R.A. (1950)	Decl. (1950)	Size (arcsec)	S_{4885} (mJy)	α	References
NGC 253	SBc	0 ^h 45 ^m 5 ^s .79	-25°33'39".1	5	820	0.84	1
NGC 520	Pec	1 21 59.62	+3 31 53.2	1	72	0.68	1
NGC 660	Sa pec	1 40 21.66	+13 23 39.8	{ 0.9 0.6 }	{ 53 41 }	0.60	1, 2
NGC 992	Sc	2 34 35.59	+20 53 4.4	3	7	0.79	1, 2
NGC 2146	Sc	6 10 41.10	+78 22 28.1	5	1
NGC 2623	Sc pec	8 35 25.28	+25 50 50.2	0.4	56	0.80	1, 2
NGC 2639	Sa	8 40 3.12	+50 23 10.1	0.2	55	0.44	1
NGC 2782	Sa pec	9 10 53.65	+40 19 15.3	0.4	40.8	0.65	1, 3
NGC 2992	Sa pec	9 43 17.62	-14 5 42.5	0.4	1
NGC 3031	Sb	9 51 27.31	+69 18 8.1	0.005	58	-0.10	1, 4, 5, 6
NGC 3079	Sc	9 58 35.01	+55 55 15.5	0.2	78	0.55	1
NGC 3504	SBb	11 00 28.53	+28 14 31.4	0.1	39	0.58	1
NGC 3690	Sc + Sc	11 25 44.18	+58 50 18.2	0.4	110	0.44	1
NGC 4102	Sb	12 3 51.22	+52 59 21.6	1	104	0.64	1
NGC 4536	Sbc	12 31 53.70	+2 27 49.7	2	49.3	0.19	1, 3, 7
NGC 4594	Sa	12 37 23.40	-11 20 54.5	<0.003	140	-0.32	1, 5, 8, 9
NGC 5236	Sc	13 34 11.10	-29 36 35.2	4	45	...	1, 3
NGC 5430	SBb	13.59 8.62	+59 34 11.1	<0.5	3.5	0.70	1, 3, 7
NGC 5635	Sb	14 26 18.86	+27 37 54.0	0.003	96	-0.65	2, 6
NGC 5675	Sb	14 30 36.63	+36 31 18.5	0.002	135	+0.1	1, 2, 6
NGC 6240	Irr	16 50 27.83	+2 28 58.5	0.5	80	0.85	1
NGC 6500	Sa	17 53 48.14	+18 20 39.8	0.003	170	0.23	2, 6
NGC 6946	Sc	20 33 49.16	+59 58 49.4	1.7	13	0.9	1
NGC 7674	Sc	23 25 24.40	+8 30 12.7	<0.3	65	1.00	2
NGC 7682	SBb	23 26 30.70	+3 15 27.7	0.3	25	0.73	2
NGC 7714	Sb	23 33 40.58	+1 52 42.1	2.1	15	0.93	1
IC 342	Sc	3 41 57.04	+67 56 28.0	2	...	0.39	1
IC 4553	Irr	15 32 46.91	+23 40 7.8	0.5	206	0.58	2
UGC 12591	Sa	23 22 54	+28 13 ...	0.009	50	...	6

REFERENCES.—(1) Condon *et al.* 1982. (2) Condon 1980. (3) van der Hulst, Crane, and Keel 1981. (4) Kellerman *et al.* 1976. (5) de Bruyn *et al.* 1976. (6) Jones, Sramek, and Terzian 1981. (7) van der Hulst and Hummel 1982. (8) Shaffer and Marscher 1979. (9) Graham, Weiler, and Wielebinski 1981.

significant), 6 cm flux, and spectral index where known. References to radio measures are also listed; van der Hulst, Crane, and Keel (1981) will be denoted hereafter by HCK. This table also lists the Hubble type for each galaxy used here, from the literature or the new plates and video camera frames described below.

b) Spectrophotometry

All galaxies in Table 1 in which the nucleus is optically accessible and for which spectrophotometry had not previously been published were observed in this study. With the exception of NGC 2146, all were observed with the image-dissector scanner (IDS) spectrographs on the 1 m Nickel or 3 m Shane reflectors at Lick Observatory or the 1.5 m Mount Lemmon telescope. Spectra were obtained in each case in the red (5400–7600 Å), and in most cases the blue (3700–6000 Å) regions at resolutions ranging from 5 to 20 Å. For NGC 2146, a slit spectrum was obtained (but not flux calibrated), using a CCD at the prime focus of the Shane telescope. Taken primarily for classification purposes, it shows that the nucleus seems to be a heavily reddened giant H II region.

Emission-line fluxes measured from these data are listed in Table 2. In nuclei with strong emission and early-type (hot) stellar continuum, no correction for underlying Balmer absorption has been applied because the H α and H β emission equivalent widths are so large in comparison to expected absorption that such a correction remains well within the measuring errors. In well-observed nuclei (NGC 660, 2639, 4102, 4594) a synthetic spectrum was generated to match those parts

of the spectrum not contaminated by emission lines with artificial populations composed of nearby stars, and subtracted to yield pure emission spectra. The emission-line fluxes were measured after application of this procedure, described in detail by Keel (1983c). The synthesis technique was also used to estimate reddenings of the stellar populations in the nuclei of NGC 660 and 4102, by varying the assumed E_{B-V} until the best spectral match was achieved. Other galaxies with weak emission and late-type stellar populations have had their H α emission fluxes corrected for stellar absorption using empirical relations between color, H α absorption equivalent width, and TiO band strength derived from synthesis of a number of spiral nuclei (Keel 1983c). The notes in Table 2 indicate which reddening and absorption corrections were applied to each spectrum.

Table 2 includes, in addition to the line fluxes, the measuring aperture (in arc seconds) and an indication of the character of the emission spectrum. The 8"1 aperture was used at the 1 m reflector, 4"7 at the 1.5 m, and 4"0 at the 3 m. Those nuclei resembling H II regions and apparently photoionized by starlight are classed as H; low-ionization spectra with [N II] λ 6584 \geq 0.7 H α are called L; and high-ionization spectra somewhat like Seyfert nuclei are coded as S. The classifications have followed the general precepts of Baldwin, Phillips, and Terlevich (1981), and are more fully described in § IIIa.

Data for classical Seyfert galaxies in the sample were taken from the literature as follows: NGC 1068, Koski 1978; NGC 3227 and 4051, Anderson 1970; NGC 4151, Anderson 1970, Antonucci and Cohen 1983, and Cohen 1983; NGC 5506, Shuder 1980; and NGC 7469, Cohen 1983. Galactic and inter-

TABLE 2
NUCLEAR EMISSION-LINE FLUXES (10^{-15} ergs cm^{-2} s^{-1})

Name	Aperture (arcsec)	H α	H β	[N II] $\lambda 6584$	[S II] $\lambda 6717, 6731$	[O I] $\lambda 6300$	[O II] $\lambda 3727$	[O III] $\lambda 5007$	$W_{\lambda}(\text{H}\alpha)$ (\AA)	$W_{\lambda}(6584)$ (\AA)	Class	Notes ^a
NGC 253	8.1	624	...	390	214	61.2	38.3	N	C
NGC 520	8.1	47.7	...	16.0	14.0	4.7	H	C
NGC 660	8.1	118	...	116	103	12.9	...	18.1	15.0	15.0	N	R, S
NGC 992	8.1	227	48	104	68	52.2	21.1	H	C
NGC 2623	8.1	22.0	...	15.0	6.7	4.6	N	C
NGC 2639	8.1	165	...	68	48	8.3	36	14.2	5.0	10.0	L/S	H α broad
NGC 2782	8.1	417	...	140	127	9.2	111	37.4	H	C
NGC 2992	8.1	713	...	258	242	22	98.4	35.6	S	C
NGC 3079	4.7	30.2	...	14.9	12.1	1.9	22.2	10.9	L	C
NGC 3504	8.1	1369	...	741	291	14.4	73.9	40.0	H	C
NGC 3690E	8.1	415	...	156	151	25.5	159	55	H	C
NGC 3690W	8.1	1636	...	511	318	40.0	259	81	H	C
NGC 4102	4.7	405	60	372	120	146	305	227	37.4	34.4	L/H	R, S
NGC 4536	4.7	204	...	98	65	45.2	21.7	H	C
NGC 4594	4.7	126	...	329	137	46	38	59	1.2	3.1	L	S
NGC 5236	4.7	1050	323	512	240	29	58	24.5	H	C
NGC 5430	4.7	133	27	56	27	5.8	22.6	...	46.3	19.5	H	C
NGC 5635	4.7	11	4.4	30	12.9	...	2.9	4.4	8.1	3.4	L	C
NGC 5675	4.7	7.6	...	10.7	17.5	6.6	3.2	...	11.9	16.7	L	C
NGC 6240	8.1	350	...	350	200	61	137	137	S	C
NGC 6500	8.1	91	...	75	111	23	32	...	14.2	11.8	L	C
NGC 6946	8.1	256	...	148	79	31.5	18.2	H	C
NGC 7674	8.1	294	...	210	75	28	68	56	S	C
NGC 7682	8.1	87	...	116	68	30	...	225	25.7	34.2	S	C
NGC 7714	9.0	1633	324	596	323	22.3	450	557	204	57	H	1
IC 342	6.0	500	101	21	15	30	...	H	2
IC 4553N	4.7	20	5.1	80
IC 4553S	4.7	6.2	31
UGC 12591	8.1	33.1	...	17.1	1.2	2.2	L	C

^a NOTES.—R = corrected for intrinsic reddening based on spectrum synthesis results. S = spectrum synthesis performed and subtracted before measurement. C = Balmer-line fluxes empirically corrected for stellar absorption features. 1 = From French 1980. 2 = From Heckman, Balick, and Crane 1980; H α extrapolated from H β , H γ .

nal reddening corrections were adopted directly from these references.

New radial velocities, with an estimated error of 200 km s^{-1} , were measured from the IDS spectra (using emission lines) for a few galaxies with no published redshift. These are NGC 660 (1100 km s^{-1} galactocentric), NGC 992 (5000 km s^{-1}), NGC 5635 (3900 km s^{-1}), NGC 6500 (3000 km s^{-1}), NGC 7682 (3250 km s^{-1}), IC 4553 (6050 km s^{-1}), and UGC 12591 (7050 km s^{-1}). More accurate values for NGC 992 and IC 4553 have recently been published by Wills and Wills (1982); their values are used here.

Spectra of representatives of H II region and low-ionization classes are shown in Figures 1 and 2. The H II region nuclei are represented by NGC 992 and 2782. Low-ionization objects shown are NGC 5635 and 5675.

c) Emission-Line Images

Fourteen of the galaxies in the samples studied here were digitally imaged through narrow-band filters to obtain pure emission-line images. Filters of FWHM 60–70 \AA on and off H α + [N II] were used, with the video camera system on the 2.1 m telescope at KPNO. The resulting image pairs were shifted to bring them into proper registration and subtracted after scaling to account for differences in filter transmission and atmospheric transparency. This was done by use of the (spectroscopically measured) equivalent widths of the lines included through a known aperture at the nucleus. The resulting maps of H α + [N II] intensity may be compared with radio and IR maps, as well as containing information on the structures of these galaxies.

Inspection of some of the images so obtained will show the power of this technique. Figure 3 (Plate 3) shows the image of the NGC 660 including H α and [N II], before and after sub-

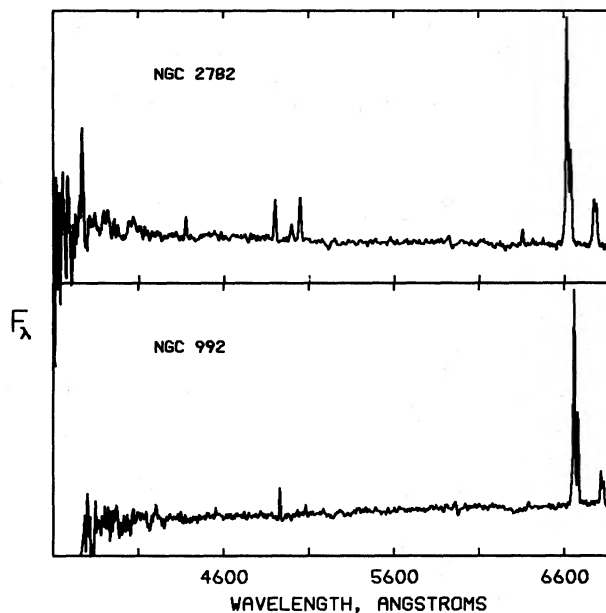
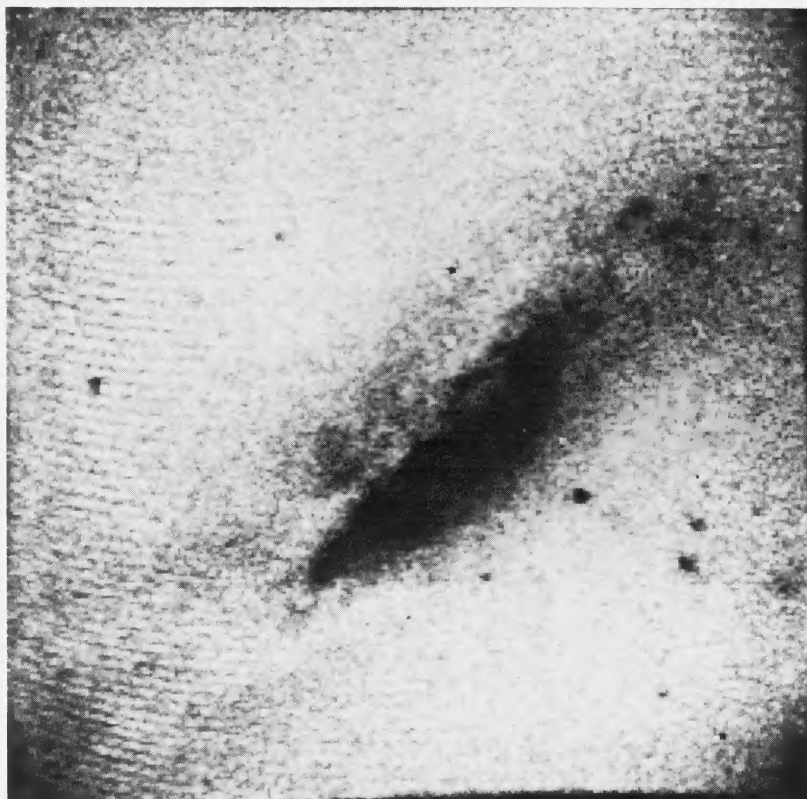
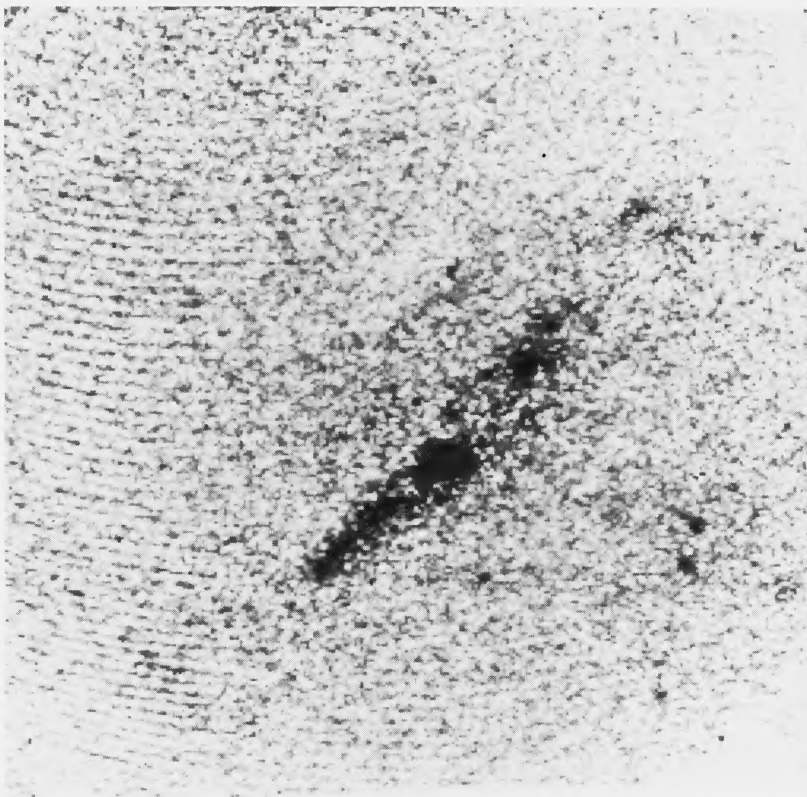


FIG. 1.—IDS spectra of galactic nuclei with H II regions: NGC 2782 and 992. Apertures were 8".1. Wavelengths are in the observed frame. The zero level is at the bottom of each frame.

NGC 660



$\lambda 6607$



$H\alpha + [N II]$

FIG. 3.—Video camera image of NGC 660 including $H\alpha$ and $[N II]$ before and after subtraction of a stellar continuum ($\lambda 6450$) image. The field is $140''$ square, with north at the top.

KEEL (see page 77)

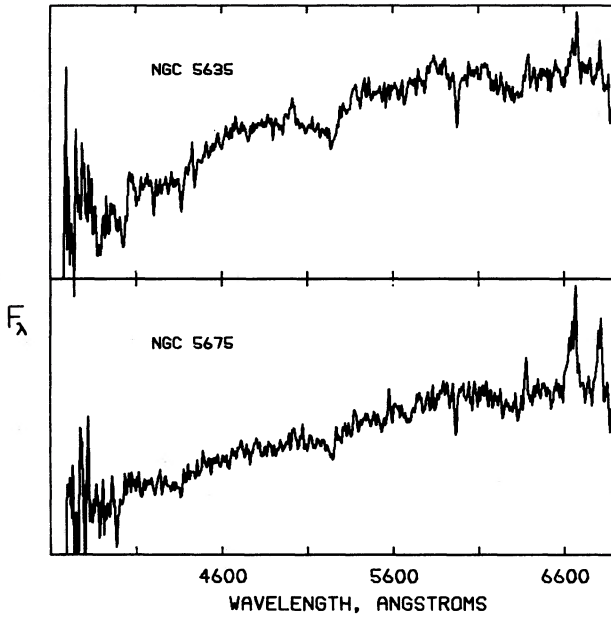


FIG. 2.—IDS spectra of low-ionization nuclei: NGC 5635 and 5675. 4"7 apertures.

traction of the 6450 Å stellar continuum image; note the dust lane and associated "bar" of H II regions.

These images were used to check on any contamination of the optical spectra by nonnuclear objects (such as inner disk H II regions), and that the line emission peaks at a point plausibly identifiable with the peak of the (stellar) continuum light distribution (this was ambiguous only in galaxies of confused structure, such as NGC 2623).

Some properties of the H α + [N II] distributions are summarized in Table 3. The full width at half-maximum and 10% of maximum are given in arc seconds and in kpc ($H_0 = 75 \text{ km s}^{-1}$). The emission-line images of those nuclei with distinct nuclear structure are shown in contour form in Figure 4. Seeing was typically 2" FWHM; this has been approximately corrected in Table 3. All plots have contour interval 10% of peak; the spatial scales vary, but each tick mark is always 0".55. The characteristic sizes of the emission regions, compared to

TABLE 3
H α + [N II] STRUCTURES IN PROGRAM NUCLEI

GALAXY	FWHM		FW AT 10%	
	arcsec	kpc	arcsec	kpc
NGC 253	8	0.13	24	0.4
NGC 520 ^a	<2	<0.3
NGC 660	4	0.3	13	0.9
NGC 992	<2	<0.6	10	3.2
NGC 2146	5	0.3	13	0.9
NGC 2623	<1.5	<0.5	11	3.8
NGC 2639	4	0.9	10	2.2
NGC 2782	6	1.0	17	2.8
NGC 4594	3	0.3	15	1.6
NGC 5430 ^b	3.5	0.7	13	2.7
NGC 7674	<2	<1.2	10	5.8
NGC 7682	<1.3	<0.3	5	1.0
NGC 7714	<1.3	<0.2	4	0.8
UGC 12591	<2	<0.9	5	2.3

^a Emission at one end of galaxy; may not represent a nucleus.

^b Extended structure or separate emission region near nucleus.

the radio dimensions in Table 1, suggest little direct connection between the ionized gas and particle distributions, except possibly in the optically unresolved (FWHM < 2") nuclei. The only detailed structural correspondence is seen in the disk H II regions in NGC 992, several of which are bright in the radio and appear in Condon's (1980) map. It appears that no detailed optical-radio relationship exists for these objects; the ionized gas distributions are much like those in spirals as a class (Keel 1983*b* and unpublished).

d) Optical Positions

In galaxies showing either optical or radio structure with scales of a few arc seconds, it is important to establish the positional correspondence between the two regimes. To this end, new positions were measured for 17 nuclei in this sample, using plates obtained with the 91 cm Crossley reflector at Lick Observatory (NGC 3690 was measured on a plate obtained with the 61 cm Baker-Schmidt telescope at Dyer Observatory). Plates were obtained for all galaxies in this study, but positions were measured only for those with more than three SAO or AGK reference stars on the plate.

Blue (103a-0 + GG13) plates were used except in the dusty galaxies NGC 253 and 660, for which red (103a-F + RG-2) plates were measured. In the case of NGC 660, the presence of two radio peaks 3" apart made an accurate optical position of enough interest to warrant a two-step procedure. In this case, an intermediate network of reference stars was set up using a wide-field plate taken with the Lick Carnegie 50 cm astrograph, and these were used as a reference system on the Crossley plate.

As might be expected, the optical and radio nuclei coincide in most galaxies. In NGC 992, 2782, 4536, 4594, 5430, 5675, 6500, and 7714 the positional agreement is within the combined (2σ) errors. The images of NGC 2623 and IC 4553 are too amorphous to determine an accurate peak; the radio emission in N2623 most nearly agrees in position with the northeastern component of the (triple) optical nucleus, while that in IC 4553/4 is nearer the center of IC 4554 (the eastern object).

The astrometry confirms the impression gained from inspection of images of N3079 that the nucleus is optically obscured; the radio source is 5".8 west and 0".9 north of the peak position of the visible bulge light, behind the prominent dust lane. Similarly, the radio emission in N0660 comes from two regions of $\sim 1".5$ extent not associated with the optical nucleus (which is at $1^{\text{h}}40^{\text{m}}21^{\text{s}}72 \pm 0.03$, $+13^{\circ}23'38".3 \pm 0".5$ in 1950 coordinates). The radio continuum arises within or behind a dust lane (see Fig. 3).

The position measures do support an identification of the central part of the optical image of N0253 as the nuclear region, as is borne out spectroscopically. The location of the radio peak (presumably at the nucleus) is shown in Figure 5 on a $\lambda 6450$ continuum isophote map.

III. IONIZATION MECHANISMS: OPTICAL AND RADIO VIEWS

a) Emission-Line Analysis and Classification

In those nuclei in which the nucleus is optically visible, a straightforward classification of the emission spectra into H II regions (defined here as nebulae photoionized by starlight), low-ionization regions, or high-ionization (Seyfert) nuclei is possible. This was done for nuclei in this sample through use of the line ratios [N II] $\lambda 6584/\text{H}\alpha$, [S II] $\lambda \lambda 6717, 6731/\text{H}\alpha$, [O I] $\lambda 6300/\text{H}\alpha$, and [O III] $\lambda 5007/\text{H}\beta$ (see Baldwin, Phillips, and Terlevich 1981). This generally yields an unambiguous result

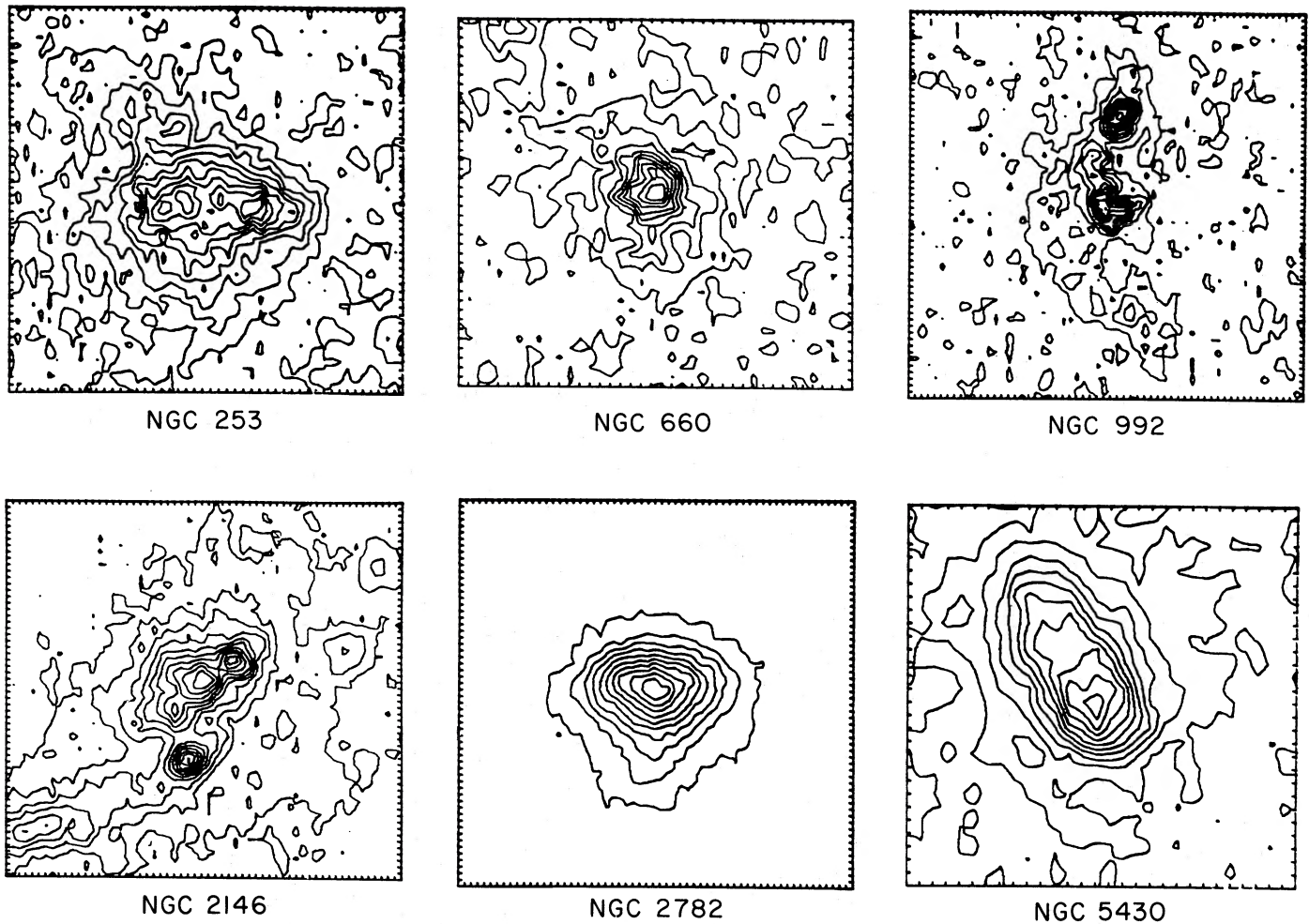


FIG. 4.—Contour representations of $H\alpha + [N II]$ images of nuclei with resolved structures above 10% of peak intensity. North is at the top, east to the left. Each tick mark is one pixel = $0''.55$. Contour interval is 10% of peak intensity.

for these nuclei; of the 33 observed here, only NGC 4102 is clearly composite (low-ionization plus $H II$ region), while the data are too poor to classify either component of IC 4553/4. NGC 2639 and 3079 show low-ionization narrow lines, but weak broad emission at $H\alpha$, indicating Seyfert activity. From

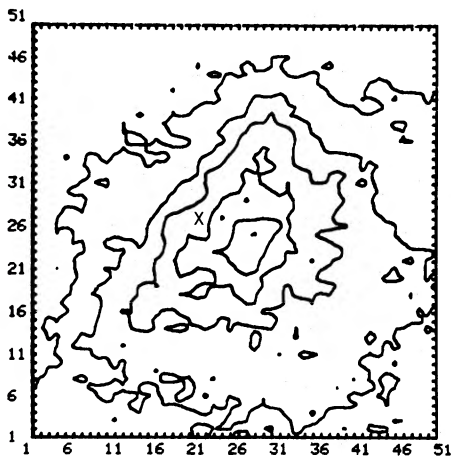


FIG. 5.—Continuum ($\lambda 6450$) isophotes of NGC 253 with the radio peak marked. North is to the left; each pixel = one tick mark = $0''.55$.

data of higher spatial resolution, Heckman *et al.* (1983) consider NGC 2782 and 3504 to be composite; with $H II$ regions and nonstellar components; for internal consistency, this analysis uses the $H II$ region classification based on the present data. The division between S and L nuclei was taken to be $[O III] \lambda 5007/H\beta = 3$, while H are divided from L and S nuclei at $[N II] \lambda 6584/H\alpha = 0.7$. Note that each of the line ratios used in these classifications spans only a small wavelength range and is thus relatively insensitive to reddening.

Before detailed examination of the emission-line ratios and luminosities in these nuclei, an instructive (and model-independent) comparison of emission-line strength is possible with the complete *optical* sample observed at $H\alpha$ and $[N II]$ by Keel (1983a). This comparison sample consists of all spirals (S0/a through Scd) with optically visible nuclei in the range $-15^\circ < \delta < +40^\circ$ and $B_T^0 < 12.0$, for a total of 93 galaxies excluding Seyferts (as the survey was published). Five Seyfert nuclei satisfy the criteria for inclusion in this sample; of these, one (NGC 4388) is very nearly edge-on and would probably have been omitted in any case if its nucleus were of normal luminosity, and three (NGC 1068, 3227, and 4151) are in common with the radio-selected sample; Seyfert data from the literature have been used to add these objects to the optical sample. An additional three non-Seyferts (NGC 660, 4536, and 4594) occur in both samples.

Direct comparison of emission-line luminosities between the optically and radio-selected samples is complicated by a correlation between minimum emission luminosity and stellar continuum luminosity (or bulge absolute magnitude) as plotted in Keel (1983a); hence the equivalent widths will be compared, since they scale very weakly with luminosity. The mean redshift of the radio sample, 2800 km s^{-1} , is much higher than that of the optical sample (1150 km s^{-1}); the difference in average angular scale between the samples was partially overcome through use of smaller projected apertures ($4''.7$) for the objects in the radio sample that are both at larger redshifts and have weaker emission, where contamination by disk H II regions could be a problem; the average linear aperture size of the radio sample (1.2 kpc) is about 30% greater than that in the optically selected sample. Thus, for emission concentrated more strongly to the nucleus than the starlight, some dilution in equivalent width might be expected in the radio sample compared to the optical one. In fact, just the opposite effect is seen (Fig. 6), showing that the *radio-selected spirals have systematically stronger emission lines than the average*. Both [N II] and H α equivalent width distributions are plotted. The [N II] distribution furnishes the cleaner test, because the H α distribution is "lumpy" and ill determined at small equivalent widths due to uncertainties in removing underlying absorption; the peak values of the [N II] distributions differ by a factor of 8. This is clear evidence of a link between unusual radio and optical properties of this sample as a whole and suggests that a more detailed exploration of optical-radio comparisons might clarify the energy sources responsible for both regimes of emission.

To perform such comparisons, intrinsic optical properties have been calculated from the observed line ratios and fluxes. Reddening correction is especially important, since the nuclear H II regions in particular show considerable internal reddening (from their Balmer decrements and stellar continua); the only low-ionization nucleus strongly affected by reddening is NGC

253 (NGC 660 is reddened but was eliminated in § II d). Reddening correction was carried out in two steps. First, all objects were corrected for the amount of galactic extinction shown in the Burstein and Heiles (1982) maps, using a standard galactic extinction curve. Then nuclei with spectroscopic indications of further extinction were corrected for this intrinsic reddening using one of several recipes. E_{B-V} for NGC 4102 was estimated to be 0.55 from the best fit spectrum synthesis among a range of trial values (Keel 1983c).

The heavily reddened nuclear H II regions present a special problem, since the observed emission lines may be weighted over the emitting volume in a manner quite different from that in which the ionizing stars or line emission are actually distributed. This problem manifests itself more strongly in line fluxes than line ratios. For comparison of optically inferred star formation rate with nonthermal radio luminosity, the required extinction measure is that which gives the H α luminosity as it would be seen in the absence of dust (so that the H α /Lyman continuum ratio would be sensibly constant). This extinction can be no smaller than that inferred from the Balmer decrement but is typically about 3 times as great in local dusty H II regions, from H β and radio free-free continuum measurements (Mathis 1983). As an estimate of the effective extinction, the mean of those two values was taken for each, with the caveat that large errors may result from the unknown geometries. Because of the large uncertainties in treating heavily reddened objects, no use is made here of line ratios spanning a large wavelength range in such cases. For two nuclei without observed H β but whose images and continuum colors suggest significant obscuration toward the nuclei, the mean extinction correction from the objects above was applied (NGC 520, 2623). One object (NGC 5236) has a measured Balmer decrement at nearly the case B recombination value.

Because the ionizing mechanisms are completely different and are expected to yield different comparisons with radio fluxes, the nuclei with gas ionized by stellar (H II regions) and nonstellar (low-ionization and Seyfert nuclei) radiation will be considered separately.

b) Nuclear H II Regions

These data can, in principle, provide a test of the hypothesis that the enhanced radio continuum in these nuclei is a direct result of present star formation (for instance, through supernova remnants as in CCGP). In normal H II regions and integrated over galactic disks, H α luminosity is an excellent indicator of star formation rate (SFR) (Kennicutt and Hodge 1980). If star-forming regions in galactic nuclei do not have important processes at work that are not seen elsewhere, a similar relation between (suitably corrected) H α and DFR should hold for star-forming nuclei. Such a relation might well have a different scaling if the initial mass function changes between disks and nuclei, but should certainly be monotonic. If H α is in fact a measure of SFR in these objects, and the enhanced radio emission comes from any mechanism which responds to SFR with a characteristic time less than the lifetime of an OB star (e.g., supernovae), a correlation between L (H α) and L (4885 MHz) should hold for this subsample. A plot of these quantities (Fig. 7) shows at most a very broad correlation with scatter of nearly an order of magnitude. While much of this scatter may be attributable to poorly determined extinction in the H α data, note that the apparent correlation depends entirely on the low-luminosity points NGC 6946 and IC 342, nuclei with little or no internal reddening. The correlation coef-

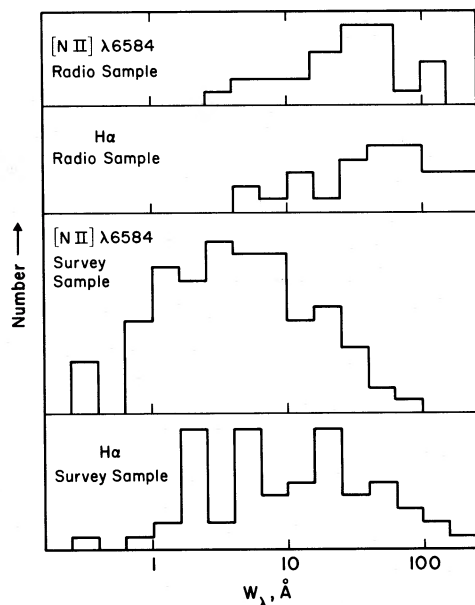


Fig. 6.—Distribution of equivalent widths (in logarithmic bins) of H α and [N II] $\lambda 6584$ for radio-selected and optically complete samples of spiral galaxy nuclei. Median aperture diameters are 1.2 kpc for radio-selected nuclei and 0.8 kpc for optically selected nuclei

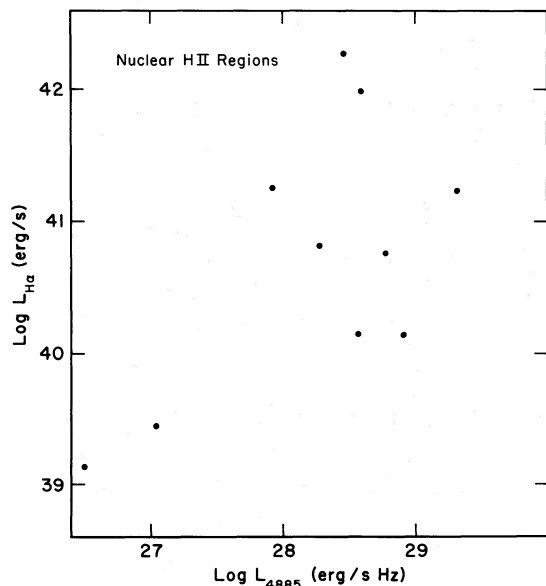


FIG. 7.—Luminosity in $H\alpha$ vs. that at 6 cm for H II region nuclei

ficient for Figure 7 is $r = 0.58$, which is only significant at the 2σ level for a sample of this size. Using corrected $H\alpha$ fluxes and 6 cm fluxes to remove distance effects yields a value of $r = -0.32$, which is tantamount to no correlation ($<1\sigma$) for this sample size. The correlation becomes worse if “minimally corrected” $H\alpha$ fluxes, using only the extinction actually implied by the Balmer decrement, are used; for fluxes, this gives $r = -0.24$.

The formal correlation coefficients show very low significance for an $H\alpha$ –6 cm flux correlation. However, it must be noted that the unknown dust distributions introduce large (and essentially unknown) errors in calculating the $H\alpha$ luminosities. Observations near $10\ \mu\text{m}$ may provide some constraints on the total dust content and its distribution in individual cases; star-forming regions that are nearly opaque at $H\alpha$ will still contribute thermal flux at $10\ \mu\text{m}$.

In the best observed cases, spectroscopic limits may be set on the fraction of the optical emission-line radiation coming from supernova remnants. Several emission-line ratios in SNR are quite distinct from the corresponding values in H II regions, resembling in many ways the low-ionization spectra discussed below. Using the filaments of the Crab (Miller 1978) and Cygnus Loop (Miller 1974) nebulae as typical of supernova remnants, the fractional contribution of such a spectrum to those observed may be estimated once assumptions about the “pure” H II region spectrum are made. Such limits can be transformed into supernova rates via the line luminosities expected for typical remnants; remnants in M31 typically have $L(H\alpha) \approx 4 \times 10^{34}$ ergs s^{-1} (Kumar 1976), which value will be used here. This of course changes with time; this test assumes a supernova rate that varies slowly compared to the lifetime of a single remnant. The most useful single line ratio for this test is $[O\ I]\ \lambda 6300/H\alpha$, with a mean of 0.25 in the SNR, but 0.02 or smaller in normal H II regions (see Baldwin, Phillips, and Terlevich 1981). The H II region nuclei in this study with detected $[O\ I]$ are NGC 2782, 3504, 3690, 5430, and 7714, with ratios $[O\ I]/H\alpha$ of 0.022, 0.022, 0.061, 0.044, and 0.014, respectively. Upper limits to the contribution from SNR can be set by assuming that they are responsible for *all* the $[O\ I]$ emission.

The resulting upper limits are $L(H\alpha) = 4L([O\ I])$ in the range 3×10^{39} – 3×10^{40} ergs s^{-1} . For typical lifetime of 5×10^4 years, these translate to upper limits on SN rate (in the optically visible area) of 1.5–15 yr^{-1} . A more realistic assumption of $[O\ I]\ \lambda 6300/H\alpha = 0.01$ in the H II regions themselves lowers these limits to the range 0.15–10 yr^{-1} . The lower end of this range is an order of magnitude below the rates quoted by CCGP; this may not be a serious problem given the uncertainties in reddening and nuclear structure, but it can provide an independent estimate of the importance of supernovae in some of these objects.

A point of interest with regard to the frequency of nuclei with high SFR is that, of the 33 galaxies in the radio-selected sample, only 11 have nuclei optically identified as photoionized by starlight. The remainder (except for IC 4553, which was not classified) are apparently powered by nonstellar sources. It is not in general the case that such nonthermal sources can be optically overwhelming evidence of star formation in these nuclei; the median $H\alpha$ luminosity is in fact higher for the H II regions, even when the luminous Seyferts such as NGC 1068 are included in the comparison. The $H\alpha/[N\ II]$ survey of Keel (1983a) suggests that it is the nuclear H II regions that can optically hide weak nonstellar activity, and not vice versa (though there is room for exceptions in the very luminous objects such as NGC 1068). These “transition” objects discussed below constitute cautionary tales for interpretation of many galactic nuclei (including our own) as being solely sites of current star formation. Even when such star formation currently powers most of the radiation at optical, infrared, and sometimes radio wavelengths, there are clearly some cases in which nonstellar activity is also present (e.g., NGC 253).

c) Nuclei with Nonstellar Ionizing Sources

The optical emission lines in Seyfert nuclei are powered by the central continuum source, and their luminosity scales with that of the central source over a wide luminosity range (Shuder 1981; Yee 1980). Recent spectroscopy has shown that the optically resolved (narrow-line) emission regions seen in some Seyferts are also photoionized by the nucleus; while contributions from hot stars are detected in NGC 1068, emission from H II regions is negligible in integrated nuclear spectra of classical Seyferts. The stellar continua of those Seyferts with weak enough featureless continua to allow detailed measurements frequently show no evidence for a significant population of young stars (Koski 1978 and Goodrich and Osterbrock 1983, for example). Therefore, for these objects, it is natural to seek a correlation between (narrow) emission-line luminosities and radio continuum luminosities (as is seen in Seyfert nuclei as a class; du Bruyn and Wilson 1978).

Detailed analysis of spectra (Keel 1983c) indicates that such an analysis is also appropriate for low-ionization nuclei (sometimes known as LINERs). Those results suggest that these objects are photoionized by low-luminosity flat-spectrum sources, essentially differing from those in Seyferts only in luminosity. Broad components at $H\alpha$ in a number of these (including NGC 2639 and 3079 in the present sample) support this contention. For these reasons, the Seyfert and low-ionization nuclei will be analyzed together.

The line luminosities are much better determined in these objects than in the H II regions, mainly because they occur in earlier Hubble-type galaxies with much less dust in their inner regions. The only low-ionization nuclei with significant reddening as found spectroscopically are NGC 253 and 660.

NGC 253 was treated in the same way as the dusty H II regions; it is worth emphasizing that the optical emission spectrum is *not* dominated by star formation, but is a low-ionization one typical of somewhat earlier type nuclei and associated with mild nonstellar activity. NGC 660 is omitted from this analysis, since the optical position indicates that both radio sources are associated with the prominent dust lane rather than the nucleus as defined by the peak of the starlight distribution. Since the low-ionization nuclei generally occur in early Hubble-type galaxies, and following the results of Keel (1983c) for this class, the other objects were corrected only for galactic reddening, as taken from Burstein and Heiles (1982). The classical Seyferts from the literature were taken to have whatever reddening was estimated by each author for the narrow-line regions. NGC 4102 is not included, since its line ratios suggest a significant contribution from a nuclear H II region (as well as dust).

The [N II] $\lambda 6584$ luminosity was selected to characterize the narrow-line region. It is preferred over that in H α because of ambiguities in separating the components of H α in nuclei with significant contributions from the broad-line region; for those cases in which a separation can be made, the [N II]/H α ratio ranges from about 0.7 to 2.0. The luminosity in [O III] $\lambda 5007$ was rejected because of a strong and systematic change in the ionization equilibrium of oxygen between high- and low-ionization nuclei, which is entirely explainable as an effect of changing ionization parameter (Ferland and Netzer 1983). This effect is much smaller, and not observed, with [N II].

As a radio-frequency parameter to correlate with [N II] luminosity, it seems appropriate to use the luminosity (at a reference frequency of 4885 MHz) of each nucleus, including either compact or resolved structures, since both kinds are presumably powered by the nuclear engine. The resulting relation is shown in Figure 8. Most of the points here define a single band, with the low-ionization objects systematically low in L [N II] (or high in L_{4885}) by about 0.4 dex. The two galaxies well off this trend are NGC 5635 and 5675; both are low-ionization nuclei with strong, compact flat-spectrum radio sources. Various individual peculiarities, such as ionized gas

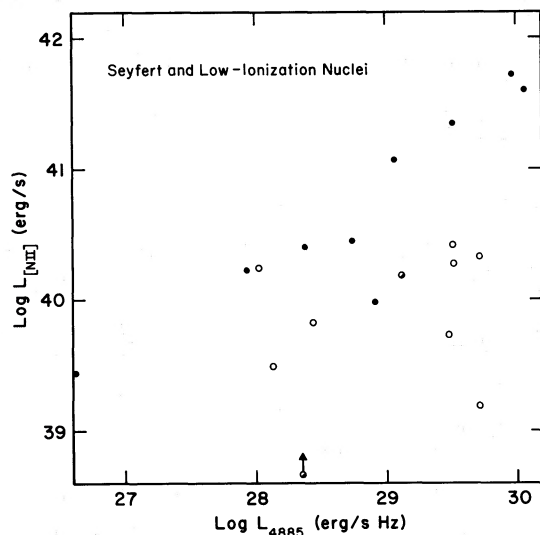


FIG. 8.—Luminosity in [N II] $\lambda 6584$ vs. that at 6 cm for Seyfert (filled circles) and low-ionization (open circles) nuclei. Transition objects (with low-ionization forbidden lines and broad H α) are shown as half-filled circles.

distributions with central “holes,” could account for this, but too little information is now available to put any such speculation on firm ground. The correlation is clear for all Seyfert and low-ionization nuclei ($r = 0.49$, significance 95%) and for the Seyferts alone ($r = 0.79$, significance $>99.5\%$). Note that the low-ionization nuclei alone do not define a very significant trend, even omitting NGC 5635 and 5675 ($r = 0.57$, significance $\sim 80\%$). The widths of the Seyfert and low-ionization loci are such that the 0.4 dex offset may not be real, given the small numbers available. The data do indicate that there is no great difference between them in [N II]-4885 MHz scaling.

The fact that both classes of nonthermally powered nuclei follow a single (broad) correlation suggests that the nonthermal sources are also responsible for the radio emission. This connection might be less direct than that with the emission-line regions; the large size range among these radio sources (FWHM from less than 4.2 pc to 250 pc) suggests that multiple emission processes are at work. The most optically luminous sources in this group have large (> 50 pc) radio sources, but it is not clear that this is significant because (a) the converse is not true (large sources do occur at all luminosities), and (b) searches for compact (VLBI) components are strongly affected by distance, both in linear resolution and in accessible flux level. Differences in emission processes are also suggested by the wide range in spectral index among these nuclei, from -0.32 (M104) to $+0.97$ (N7674). The very-flat-spectrum sources are reasonably well understood as compact, self-absorbed synchrotron sources, but the relation between steep-spectrum emission and active nuclei may take one of several forms. Note that all the radio sources with very small components (~ 5 pc FWHM) occur in low-ionization (six) or Seyfert (three) nuclei.

The presence of several compact, presumably synchrotron self-absorbed sources in this group suggests that the others might be aging or expanding counterparts, with steeper spectra due to energy losses in single particle bursts or decreasing opacity at centimeter wavelengths. This picture makes the sources in nonthermally active spiral nuclei close (weaker) analogs of the central sources in radio galaxies and QSOs. Such a conclusion is in accord with the optical interpretation of the emission spectra of these objects as being produced by nonthermally radiating central objects.

Because the physical environment in the nucleus of a spiral is quite different from that in a typical (elliptical) radio galaxy, less direct models may also apply. It is possible that, in some objects, the radio sources may be powered by starbursts (e.g., through supernova remnants). This possibility will be discussed more fully later in connection with composite nuclei. Interaction of jets or beams with the interstellar medium in a disk galaxy also seems to produce particle acceleration, as discussed for 3C 305 by Heckman *et al.* (1982). As those authors note, energy transport by bulk motion (ejected plasma blobs or more continuous jets) can produce *in situ* particle acceleration and subsequent radio emission under local physical conditions that are very similar to those in supernova remnants; thus the integrated properties of such a radio source might well mimic those of an ensemble of SNR. It is not clear in the general case whether the optical spectrum would more closely resemble that of shocked or photoionized gas, since both processes (plus photoionization caused by the UV lines emitted by the shocked gas, as in the models by Shull and McKee 1979) would be occurring.

The scheme proposed by de Bruyn and Wilson (1978), in

which the relation between forbidden-line and radio luminosities is accounted for by rough pressure balance between the optically emitting gas (filling factor $\sim 10^{-4}$) and the particles plus magnetic field responsible for radio emission (filling factor near unity) may reasonably be invoked for all the nonthermal nuclei in this sample. A third component, hot low-density gas, is predicted by galactic wind models (Mathews and Baker 1971; Faber and Gallagher 1978; Bregman 1978). Predicted temperatures (10^7 K) and densities (1.0 cm^{-3}) for this component would put it in rough pressure balance with the other two; large variations in the filling factor of hot gas could produce the range of $H\alpha/6 \text{ cm}$ ratios observed. The X-rays from such a gas would be detectable at a sensitivity about 10 times that of the *Einstein* IPC.

Such a picture would require the forbidden-line regions and extended radio structures to be roughly coextensive. Too few of the low-ionization nuclei in this sample have been imaged in $H\alpha + [N \text{ II}]$ to test this on the radio sample, but these and optically similar nuclei have nuclear emission-line extents typically of a few hundred parsecs (Keel 1983*b*) in broad accord with expectation. A similar situation holds in Seyferts (Wilson 1979).

Several kinds of observations can clarify the situation in these nuclei. Multifrequency radio maps of high enough quality to permit construction of high-resolution spectral index maps might allow spatial separation of various emission processes in complex situations, and separate nonthermal contributions when both are present; this has in fact been done by Turner and Ho (1983) for NGC 253. Similarly, optical spectroscopy at higher spatial resolutions can separate various emission mechanisms and search for the velocity structure expected if significant kinetic energy transport is occurring (Heckman *et al.* 1982) and tell whether enough star formation is occurring near the nuclei to affect ionization conditions and energetics. Finally, observations of optically complete samples in the radio will give a more representative view of events in these nuclei.

d) Composite Nuclei: The Chicken or the Egg?

There are some nuclei in this sample that show evidence, from the optical data alone, of both nonthermal activity and recent star formation. From the basic standpoint of understanding processes in galactic nuclei, it is important to know whether these two conditions are causally related, and if so in which direction and by what mechanisms.

Evidence for such composite objects is afforded by nuclei in which the optical and radio classification (stellar vs. nonstellar and compact vs. extended, or flat-vs.-steep-spectrum) suggest different mechanisms. Such objects include NGC 253, 2782, and 3504. The optical spectrum of that part of the nucleus of NGC 253 which is visible suggests nonstellar photoionization, while abundant radio and infrared data point toward massive star formation near the nucleus (CCGP; Becklin, Fomalont, and Neugebauer 1973). In the other two cases, the optical spectra are dominated by the star formation, while the radio sources are as small as can be measured at the VLA and have flatter spectra than any of the other H II region nuclei.

Active nuclei and H II regions are known to exist in close proximity in a number of galaxies. In NGC 1365, a relatively inconspicuous Seyfert nucleus sits among several (optically) more luminous H II regions (Edmunds and Pagel 1982). Many "hot-spot" galaxies have nuclei (coinciding with the central peak of starlight intensity) that show the kind of low-ionization

emission interpreted here as resulting from dilute power-law photoionization, surrounded by rings of H II regions; some examples are NGC 1097, 4303, and (over a larger scale) 4736. Radio maps of such objects (such as NGC 2903 and 4736 in HCK) show that the H II regions can also be the most prominent features at centimeter wavelengths. Such situations account for the dichotomy between optical and radio classifications of some nuclei.

Little direct information is yet available on any causal relation between the nuclear starbursts and the active nuclei. Weedman (1983) has noted that the remnants of a starburst can sink rapidly into a very compact configuration which, under some conditions, could form a single massive object such as seems necessary to power active nuclei. The massive object would be permanent, unlike obvious evidence of the starburst; it would be formed after the first burst of nuclear star formation and coexist with any subsequent ones. This scenario would have starbursts as the original cause of all kinds of unusual nuclear events.

An alternative view suggests that an active nucleus may induce nearby star formation, through shocks or less violent cloud compressions produced by rapid bulk motion in the immediate vicinity of the nucleus or ejected matter. This has been proposed to account for the early spectral type of starlight seen around some QSOs (Boroson and Oke 1982; Balick and Heckman 1983). Association of large numbers of hot stars with an active nucleus also appears in the N galaxy 3C 459 (Miller 1981). In less extreme systems, Yee (1983) finds evidence that the starlight very close to Seyfert I nuclei is bluer than expected for the galaxies' morphological types. At present, such work is strongly hampered by scattered (blue) nuclear light; photometry or spectroscopy with high spatial resolution will be required to separate these effects. Useful limits on young stellar populations in Seyfert nuclei are difficult to set with available spectra because in the absence of measurable Balmer absorption (due to filling by emission) the blue stellar continuum is almost impossible to separate from the featureless continuum over the available wavelength range (Goodrich and Osterbrook 1983). This could be remedied by accurate UV spectrophotometry in those objects where the nuclear continuum does not completely swamp the starlight. These nuclei are potentially quite important in addressing the questions above, as firm examples of the coexistence of exotic and stellar phenomena in a single nucleus.

IV. CONCLUSIONS

Optical spectrophotometry of a sample of radio-selected spiral galaxy nuclei has been used to determine the mechanism responsible for optical emission lines in each case and examine the relationships between emission-line and 6 cm luminosities for various emission-line classes. The star-forming (H II region) nuclei do not show an expected correlation between reddening-corrected $H\alpha$ luminosity and radio continuum luminosity. The optical spectra allow limits on the number of supernova remnants *optically visible* in each nucleus which in some cases yield average supernova rates below those necessary to account for the radio emission uncertainties; in reddening make this test inconclusive.

Treated as a single class, Seyfert and low-ionization nuclei show some correlation between emission-line and 6 cm luminosities, tighter for the Seyferts alone. This is interpreted as evidence for a single nonthermal source powering the optical emission region and (in some cases indirectly) the radio emis-

sion. Both optical spectra and disagreements between optical and radio classifications suggest that a number of these nuclei are composites with significant energy output from flat-spectrum compact sources and young stars. Further study of these nuclei will be important in clarifying whether the phenomena are causally related, and if so in which direction.

I am grateful to Dr. Joe Miller for providing the 3 m telescope time. Drs. Jim Condon and Thijs van der Hulst provided data in advance of publication. Ed Carder introduced me to

the KPNO Grant machine, and Dr. Burt Jones gave me a timely position reduction program. The National Science Foundation supported this work through a graduate fellowship during a portion of this study and is supporting IDS observations on Mount Lemmon under a grant to the University of California at San Diego. Conversations with Drs. Tim Heckman and Dave De Young were helpful, as were the comments of the referees who forced me to sharpen some fuzzy points in the analysis.

REFERENCES

- Anderson, K. S. 1970, *Ap. J.*, **162**, 743.
 Antonucci, R. R. J., and Cohen, R. D. 1983, *Ap. J.*, **271**, 564.
 Baldwin, J., Phillips, M. M., and Terlevich, R. 1981, *Pub. A.S.P.*, **93**, 5.
 Balick, B., and Heckman, T. M. 1983, *Ap. J. (Letters)*, **265**, L1.
 Becklin, E. E., Fomalont, E. B., and Neugebauer, G. 1973, *Ap. J. (Letters)*, **181**, L27.
 Boroson, T. A., and Oke, J. B. 1982, *Nature*, **296**, 397.
 Bregman, J. N. 1978, *Ap. J.*, **224**, 768.
 Burstein, D., and Heiles, C. 1982, *A.J.*, **87**, 1165.
 Cohen, R. D. 1983, *Ap. J.*, **273**, 489.
 Condon, J. J. 1980, *Ap. J.*, **242**, 894.
 Condon, J. J., Condon, M. A., Gisler, G., and Puschell, J. J. 1982, *Ap. J.*, **252**, 102 (CCGP).
 de Bruyn, A. G., Crane, P. C., Price, R. M., and Carlson, J. B. 1976, *Astr. Ap.*, **46**, 243.
 de Bruyn, A. G., and Wilson, A. S. 1978, *Astr. Ap.*, **64**, 433.
 Edmunds, M. G., and Pagel, B. E. J. 1982, *M.N.R.A.S.*, **198**, 1089.
 Faber, S. M., and Gallagher, J. S. 1976, *Ap. J.*, **204**, 365.
 Ferland, G. J., and Netzer, H. 1983, *Ap. J.*, **264**, 105.
 French, H. B. 1980, *Ap. J.*, **240**, 41.
 Gehrz, R. D., Sramek, R. A., and Weedman, D. W. 1983, *Ap. J.*, **267**, 551.
 Goodrich, R. W., and Osterbrock, D. E. 1983, *Ap. J.*, **269**, 416.
 Graham, D. A., Weiler, K. W., and Wielebinski, R. 1981, *Astr. Ap.*, **97**, 388.
 Heckman, T. M., Balick, B., and Crane, P. C. 1980, *Astr. Ap. Suppl.*, **40**, 295.
 Heckman, T. M., van Breugel, W. J. M., Miley, G. K., and Butcher, H. R. 1983, *A.J.*, **88**, 1077.
 Heckman, T. M., Miley, G. K., Balick, B., van Breugel, W. J. M., and Butcher, H. R. 1982, *Ap. J.*, **262**, 529.
 Hummel, E. 1980, *Astr. Ap.*, **96**, 111.
 Jones, D. C., Sramek, R. A., and Terzian, Y. 1981, *Ap. J.*, **246**, 28.
 Keel, W. C. 1983a, *Ap. J. Suppl.*, **52**, 229.
 ———. 1983b, *Ap. J.*, **268**, 632.
 ———. 1983c, *Ap. J.*, **269**, 466.
 Kennicutt, R. C., Jr., and Hodge, P. W. 1980, *Ap. J.*, **241**, 573.
 Kellermann, K. I., Shaffer, D. B., Pauliny-Toth, I. I. K., Preuss, E., and Witzel, A. 1976, *Ap. J. (Letters)*, **210**, L121.
 Koski, A. T. 1978, *Ap. J.*, **223**, 56.
 Kumar, C. K. 1976, *Pub. A.S.P.*, **88**, 323.
 Mathews, W. G., and Baker, J. C. 1971, *Ap. J.*, **170**, 241.
 Mathis, J. S. 1983, *Ap. J.*, **267**, 119.
 Miller, J. S. 1974, *Ap. J.*, **189**, 239.
 ———. 1978, *Ap. J.*, **220**, 490.
 ———. 1981, *Pub. A.S.P.*, **93**, 681.
 Rickard, L. J., Bania, T. M., and Turner, B. G. 1982, *Ap. J.*, **252**, 147.
 Shaffer, D. B., and Marscher, A. P. 1979, *Ap. J. (Letters)*, **233**, L105.
 Shuder, J. M. 1980, *Ap. J.*, **240**, 32.
 ———. 1981, *Ap. J.*, **244**, 12.
 Shull, J. M., and McKee, C. F. 1979, *Ap. J.*, **227**, 131.
 Turner, J. L., and Ho, P. T. P. 1983, *Ap. J. (Letters)*, **268**, L79.
 van der Hulst, J. M., Crane, P. C., and Keel, W. C. 1981, *A.J.*, **86**, 1175 (HCK).
 van der Hulst, J. M., and Hummel, E. 1982, private communication.
 Weedman, D. W. 1983, *Ap. J.*, **216**, 479.
 Wills, P., and Wills, B. J. 1982, *A.J.*, **87**, 252.
 Wilson, A. S. 1979, *Proc. Roy. Soc. London A*, **366**, 461.
 Yee, H. C. K. 1980, *Ap. J.*, **241**, 894.
 ———. 1983, *Ap. J.*, **272**, 473.

WILLIAM C. KEEL: Kitt Peak National Observatory, P.O. Box 26732, Tucson, AZ 85726-6732